

# Adaptation of uncertainty-penalized Bayesian information criterion for parametric partial differential equation discovery

**Pongpisit Thanasutives**

*Graduate School of Information Science and Technology, Osaka University, Osaka, Japan*

THANASUTIVES@AI.SANKEN.OSAKA-U.AC.JP

**Ken-ichi Fukui**

*SANKEN (The Institute of Scientific and Industrial Research), Osaka University, Osaka, Japan*

FUKUI@AI.SANKEN.OSAKA-U.AC.JP

## Abstract

Data-driven discovery of partial differential equations (PDEs) has emerged as a promising approach for deriving governing physics when domain knowledge about observed data is limited. Despite recent progress, the identification of governing equations and their parametric dependencies using conventional information criteria remains challenging in noisy situations, as the criteria tend to select overly complex PDEs. In this paper, we introduce an extension of the uncertainty-penalized Bayesian information criterion (UBIC), which is adapted to solve parametric PDE discovery problems efficiently without requiring computationally expensive PDE simulations. This extended UBIC uses quantified PDE uncertainty over different temporal or spatial points to prevent overfitting in model selection. The UBIC is computed with data transformation based on power spectral densities to discover the governing parametric PDE that truly captures qualitative features in frequency space with a few significant terms and their parametric dependencies (i.e., the varying PDE coefficients), evaluated with confidence intervals. Numerical experiments on canonical PDEs demonstrate that our extended UBIC can identify the true number of terms and their varying coefficients accurately, even in the presence of noise. The code is available at <https://github.com/Pongpisit-Thanasutives/parametric-discovery>.

**Keywords:** data-driven discovery; information criterion; model selection; partial differential equation; SINDy; uncertainty quantification.

## 1. Introduction

The field of data-driven partial differential equation (PDE) discovery has been advanced progressively with the objective of identifying the governing PDE of a dynamical system automatically. Unlike the traditional derivation of physics from first principles, the data-driven discovery method leverages machine learning techniques applied directly to observed data to achieve greater flexibility and accuracy, as statistical or deep models are tailored to the intricacies of the observed data. A sparse regression based method like SINDy (sparse identification of nonlinear dynamics) (Brunton et al., 2016; Rudy et al., 2017) is typically used to discover nonlinear dynamics, described by a differential equation, via approximating the temporal derivative of a system’s state variable using a linear combination of candidate terms. Successful applications of SINDy have been shown in various domains, including but not limited to aerodynamics, biology, and epidemiology (Ghadami and Epureanu, 2022).

Throughout the evolution of the field, significant challenges have arisen as primary concerns in the development of data-driven PDE discovery methods. One major challenge that cannot be resolved trivially is determining the optimal regularization hyperparameter(s) for sparse regression. Improper hyperparameter tuning can easily lead to incorrect models, either overfitted or underfitted. To address this issue, PDE discovery methods based on best-subset selection (Bertsimas and Gurnee, 2023) have been introduced, offering customizable sparsity in regression models (i.e., the number of nonzero terms or the support size). Nevertheless, these methods sacrifice training speed for greater control over sparsity and the precision of effective candidate terms.

Suppose we have obtained correct support sets that represent potential PDEs of different complexity measures. The model selection step is still required to determine the optimal support size, commonly using an information criterion. In other words, we must decide how many candidate terms should be included in the underlying physics. Conventional criteria like Akaike and Bayesian information criteria (AIC/BIC) (Akaike, 1974; Schwarz, 1978), despite being widely used in various scientific disciplines, struggle to select the optimal support size for the governing equation, favoring overly complex models, when no PDE simulation is performed before the AIC calculation (Thanasutives et al., 2023). In contrast to SINDy-AIC (Mangan et al., 2017), which necessitates simulations of multiple potential PDEs before calculating AIC scores, we are more interested in achieving reliable and fast model selection without requiring any PDE solutions. As discussed by Rudy et al. (2019) and Dong et al. (2023), minimizing AIC with a variable threshold benchmark or tolerance can lead to selecting an incorrect governing PDE. Setting the threshold too low results in an overly sparse PDE, while setting it too high leads to an overfitted PDE. Following Ockham’s razor, the uncertainty-penalized information criterion (UBIC) (Thanasutives et al., 2024; Thanasutives and Fukui, 2024) has been recently proposed to balance model accuracy and complexity while accounting for PDE uncertainty. UBIC incorporates the quantified uncertainty of PDE coefficients (model parameters) to avoid overfitting. The PDE uncertainty is achieved by employing Bayesian regression to infer posterior distributions of the coefficients, from which the mean and covariance are computed. The resulting coefficient of variation penalizes the base BIC adaptively to ensure the selection of a parsimonious and stable equation as the governing PDE. Different from UQ-SINDy (Hirsh et al., 2022), which quantifies the uncertainty of PDE coefficients (sparsified by priors) but does not make use of this uncertainty to impact model selection, UBIC employs its quantified uncertainty to address the overfitting problem.

The central challenge of this paper is to find the number of spatially or temporally varying coefficients in the governing parametric equation. In cases where the PDE coefficients are not just constant, the governing PDE identification becomes much more difficult. The aforementioned methods were originally proposed to tackle the PDE discovery problem with constant coefficients but are unable to handle varying coefficients.

To discover parametric PDEs, Rudy et al. (2019) proposed sequential grouped threshold ridge regression (SGTR), where a separate sparse regression is solved for each time step (or spatial point for the case of spatially dependent PDEs) to attain corresponding time-varying coefficients. Although this method is able to obtain coefficients for each specific point, it cannot provide a symbolic expression for varying coefficients. SGTR relies on AICc (AIC with a correction for small sample sizes) (Hurvich and Tsai, 1989) losses, which do not pro-

mote parsimonious PDEs and thus probably mislead us into selecting unnecessarily complex PDEs. Moreover, the SGTR algorithm is noise-intolerant, which may result in discovering an incorrect PDE form or structure. We refer readers to [Li et al. \(2020\)](#) for an extended SGTR with double low-rank decompositions (to denoise sparse outlying entries) and to [Luo et al. \(2023\)](#) for a kernelized SGTR that improves noise robustness, albeit at the increased computational cost. Although these methods have shown noise robustness, their model selection relies on either tweaking the amount of norm-based regularization applied or using AIC with costly PDE simulations. [Xu et al. \(2021\)](#) tackled parametric PDE discovery problems using DLGA-PDE, a genetic algorithm-based framework that employs deep learning as a mesh-free function approximator. Although the framework can discover the governing parametric PDE in closed form, giving symbolic expressions for varying coefficients, the PDE structure identification step is computationally intensive because of the need to train neural networks repeatedly on different PDEs found during the genetic algorithm’s learning process. Furthermore, tuning the regularization hyperparameters in the fitness function is problematic because it depends on (biased) human experience, making the identification process difficult to automate, as discussed earlier.

Our main contribution is the new extension of UBIC, adapted to solve parametric PDE discovery problems. This extended UBIC leverages quantified PDE uncertainty as a complexity penalty to address the overfitting issue in the model selection step. It also inherits the benefits of UBIC, including no computationally expensive PDE simulation required (low computational resource requirements) and minimal dependence on hyperparameter tuning (see [Thanasutives et al., 2024](#)). We find that using the UBIC score of the power spectral densities of the regression model and the temporal derivative effectively prevents the selection of overfitted PDEs, promoting the parsimonious model that truly captures qualitative features in frequency space. As a byproduct of computing the UBIC, we provide confidence intervals for all coefficients, each evaluated at a particular time step or spatial grid point.

## 2. Methodology

### 2.1. Problem Formulation

Let us consider the following parametric form of governing partial differential equations:

$$u_t = \mathcal{N}(u, u_x, u_{xx}, \dots; \mu(x, t)) = \sum_{j=1} \mathcal{N}_j(u, u_x, u_{xx}, \dots) \mu_j(x, t). \quad (1)$$

We aim to identify the nonlinear operator  $\mathcal{N}$ , which involves spatial derivatives of the state variable  $u$ , whose realization  $\mathbf{U} \in \mathbb{R}^{N_x \times N_t}$  is given in a spatio-temporal grid.  $\mathcal{N}$  is parameterized by  $\mu(x, t)$ , reducible to either  $\mu(x)$  or  $\mu(t)$ —spatially or temporally varying functions.

### 2.2. Sparse Regression

Suppose, without loss of generality to spatially varying cases, Equation (1) can be formulated as systems of linear equations, with temporal dependency. Given there are  $N_t$  time steps and  $N_x$  spatial points, the system evaluated at a time  $t_i$  is expressed by

$$\mathbf{U}_t^i = \mathbf{Q}^i \boldsymbol{\xi}^i = \sum_{j=1}^{N_q} \xi_j^i \mathbf{q}_j^i; \quad \mathbf{Q}^i = \begin{pmatrix} | & & | & & | \\ \mathbf{q}_1^i & \cdots & \mathbf{q}_j^i & \cdots & \\ | & & | & & | \end{pmatrix} \in \mathbb{R}^{N_x \times N_q}. \quad (2)$$

$\mathbf{U}_t$  is the time derivative numerically computed with Kalman smoothing. Every  $\mathbf{Q}^i$  comprises the identical  $N_q$  candidate terms, which are presumed overcomplete, with each term possibly appearing in the true  $\mathcal{N}$ . We define the candidate library  $\mathbf{Q}$  as a block-diagonal matrix constructed by all  $\mathbf{Q}^i$  matrices, deriving a single system for the parametric PDE discovery problem:  $\mathbf{U}_t = \mathbf{Q}\boldsymbol{\Xi}$ . We achieve the best-subset solution with  $s_k$  support size via solving the sparse regression separately for each time step:

$$\hat{\boldsymbol{\Xi}} = \min_{\boldsymbol{\Xi}} \sum_{i=1}^{N_t} \left\| \mathbf{U}_t^i - \mathbf{Q}^i \boldsymbol{\xi}^i \right\|_2^2 + \lambda \left\| \boldsymbol{\xi}^i \right\|_2^2, \text{ such that } \left\| \boldsymbol{\xi}^i \right\|_0 = s_k, \forall i \leq N_t; \quad (3)$$

where  $\mathbf{U}$  and  $\mathbf{Q}$  are the validation data on which  $\boldsymbol{\Xi} \in \mathbb{R}^{N_q \times N_t}$  is evaluated. The best-subset solver based on mixed-integer optimization (MIOSR) (Bertsimas and Gurnee, 2023) is used to gather  $\boldsymbol{\xi}^i$  of consecutive support sizes with  $\lambda = 0$ . Note that MIOSR is preferred here over SGTR to ensure that potential PDEs with certain support sizes are not overlooked. We can impose the group sparsity in  $\boldsymbol{\Xi}$  by controlling that the support set  $\{j \mid |\xi_j^i| > 0\}, \forall i \leq N_t$  is the same for every time step. Remark that the group sparsity condition is not necessary before optimizing for the optimal number of nonzero terms (support size)  $s^* \in \{s_k \mid k = 1, 2, \dots\}$ . Because we cannot infer  $s^*$  solely from Equation (3), and the model selection step is performed next.

### 2.3. Model Selection

We minimize an information criterion to select the optimal support size  $s^*$ . An information criterion is usually expressed by

$$-2 \log L(\hat{\boldsymbol{\Xi}}) + \mathcal{C}(a_N, \hat{\boldsymbol{\Xi}}, \mathcal{P}); \quad (4)$$

where  $L$  is the likelihood function, and  $\mathcal{C}(a_N, \hat{\boldsymbol{\Xi}}, \mathcal{P})$  is the complexity penalty corresponding to the criterion. For example,  $2s_k$  and  $\log(N)s_k$ ; where  $N = N_x N_t$ , is the complexity penalty for AIC and BIC, respectively. We regard  $\mathcal{P}$  as any other necessary information, e.g., the complexity measures of ICOMP (informational complexity criterion) (Bozdogan and Haughton, 1998) or the UBIC's quantified PDE uncertainty. Considering a particular support size  $s_k$ , the extension of the original UBIC (incorporating a fixed threshold  $\zeta = 10^{-5}$  to prevent underflowing) is proposed for parametric PDE discovery as follows:

$$\text{UBIC}_k = N \log \left( \frac{2\pi \left\| \mathbf{U}_t - \mathbf{Q}\hat{\boldsymbol{\Xi}} \right\|_2^2}{N} + \zeta \right) + \log(N)(\mathfrak{U} + s_k); \quad (5)$$

$$\mathfrak{U} = 10^{\lambda^*} \bar{V}, \quad \bar{V} = \frac{V}{V_{\max}}, \quad V = \sum_{i=1}^{N_t} R_i, \quad \text{and } R_i = \frac{\sum_{j=1}^{s_k} \sigma_j^i}{\left\| \boldsymbol{\xi}^i \right\|_1}.$$

According to [Thanasutives et al. \(2024\)](#), we compute the uncertainty  $\mathfrak{U}$  (of the  $s_k$ -support-size PDE) using the tuned data-dependent  $\lambda^*$  and the scaled coefficient of variation  $\bar{V}$ . At each time step,  $V$  accumulates an instability ratio  $R_i$  of the total posterior standard deviation and the coefficient vector L1-norm, both obtained by applying Bayesian automatic relevance determination (ARD) regression ([MacKay et al., 1994](#)).  $V_{\max}$  is the maximum value of  $V$  over all available support sizes. Essentially with the temporal (or spatial) accumulation, we can extend the original UBIC for parametric PDE discovery. Remark that if we weaken the group sparsity assumption, we allow each  $\hat{\xi}^i$  to have a unique support set— $S^i = \{j \mid \hat{\xi}_j^i \neq 0\}$  with an equal support size (cardinality)  $|S^i| = s_k$ , leading to a reasonable increase in the complexity penalty simply by considering  $s_k \times |\{S^i\}|$  instead of just having a  $s_k$  fixed across the temporal or spatial axis.

**Power spectral density based transformation.** The validation data  $\mathbf{Q}$  in frequency space is obtained by applying discrete Fourier transformation along the temporal axis to every

$$\mathbf{Q}_j = \begin{pmatrix} | & | & | & | \\ \mathbf{q}_j^1 & \cdots & \mathbf{q}_j^i & \cdots \\ | & | & | & | \end{pmatrix} \in \mathbb{R}^{N_x \times N_t},$$

and removing entries that correspond to low-power frequencies—less than the ninety percentile. The transformation technique is not only beneficial when deciding the optimal coefficient vector with  $s_k$  support size, but also when selecting the optimal  $s^*$ . More specifically, we generalize the residual sum of squares (RSS) to  $\left\|T(\mathbf{U}_t) - T(\mathbf{Q}\hat{\Xi})\right\|_2^2$ ; where  $T$  denotes a function, which transforms  $\mathbf{U}_t$  and  $\mathbf{Q}\hat{\Xi}$  to new representations, i.e., mapping  $T(\mathbf{U}_t) = \tilde{\mathbf{U}}_t$ . In this work, every  $\tilde{\mathbf{U}}_t^i$  is a numerical result from a trapezoidal integration applied along the spatial axis (the frequency/temporal axis for a spatially dependent PDE) of estimated power spectral density (PSD) using a periodogram (see `scipy.integrate.trapezoid` and `scipy.signal.periodogram`). The PSD representation is a good choice because of its clear characteristics (see Appendix B), which exhibits larger values for true data-generating frequencies ([Welch, 1967](#)). The integration trick is to limit the sample number, and therefore facilitates the model selection step, as it is known that conventional information criteria tend to select overfitted PDEs when the number of samples is large ([Thanasutives et al., 2023, 2024](#)). The integration is ablated if the estimated PSD is already a one-dimensional vector.

**Support size filtering.** When tuning for  $\lambda^*$  to ultimately achieve  $s^*$ , we only consider a sequence of significant support sizes  $[k \mid \text{BIC}_k < \text{BIC}_{k'} \wedge p_{\text{MW}}([\text{BIC}_k^i], [\text{BIC}_{k'}^i]) < p_{\text{cut}}]$ ; where  $k' = \arg \min_{k' < k} \text{BIC}_{k'}$ . We refer to  $[\text{BIC}_k^i]$  as a collection of temporally varying BIC scores, each calculated on  $T(\mathbf{U}_t^i)$  and  $T(\mathbf{Q}^i \hat{\xi}^i)$ .  $p_{\text{MW}}([\text{BIC}_k^i], [\text{BIC}_{k'}^i])$  is the p-value resulted from the Mann–Whitney test with the alternative hypothesis stating that the distribution underlying  $[\text{BIC}_k^i]$  is stochastically less than the distribution underlying  $[\text{BIC}_{k'}^i]$ , hence the significant improvement by increasing the support size from  $s_{k'}$  to  $s_k$ . The median of  $\{p \mid p = p_{\text{MW}}([\text{BIC}_{k+1}^i], [\text{BIC}_k^i]) \wedge p < 0.01\}$  defines  $p_{\text{cut}}$ , ensuring that we consider only the top improvements with at least 99% confidence. We recommend researchers explore a generalized percentile-based notion beyond sticking to the strict median.

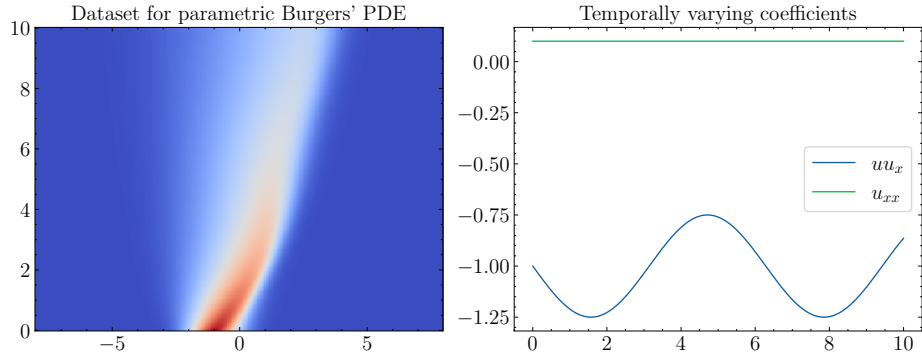


Figure 1: Visualization of the state variable and the temporally varying coefficients for the parametric Burgers' PDE dataset.

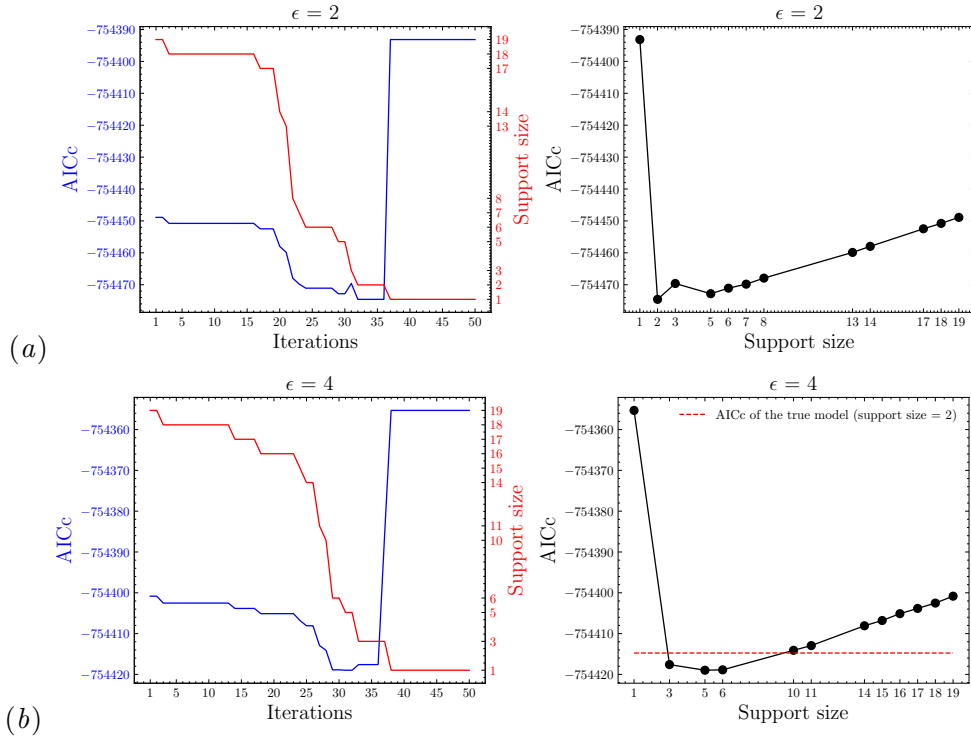


Figure 2: **Parametric Burgers' PDE**: Model selection using AICc employed by the SGTR algorithm under noisy situations. According to Rudy et al. (2019), RSS is calculated based on every L2-normalized  $U_t^i$  and  $Q^i$ .

### 3. Numerical Experiments

The code for reproducing our results is available at <https://github.com/Pongpisit-Thanasutives/parametric-discovery>.

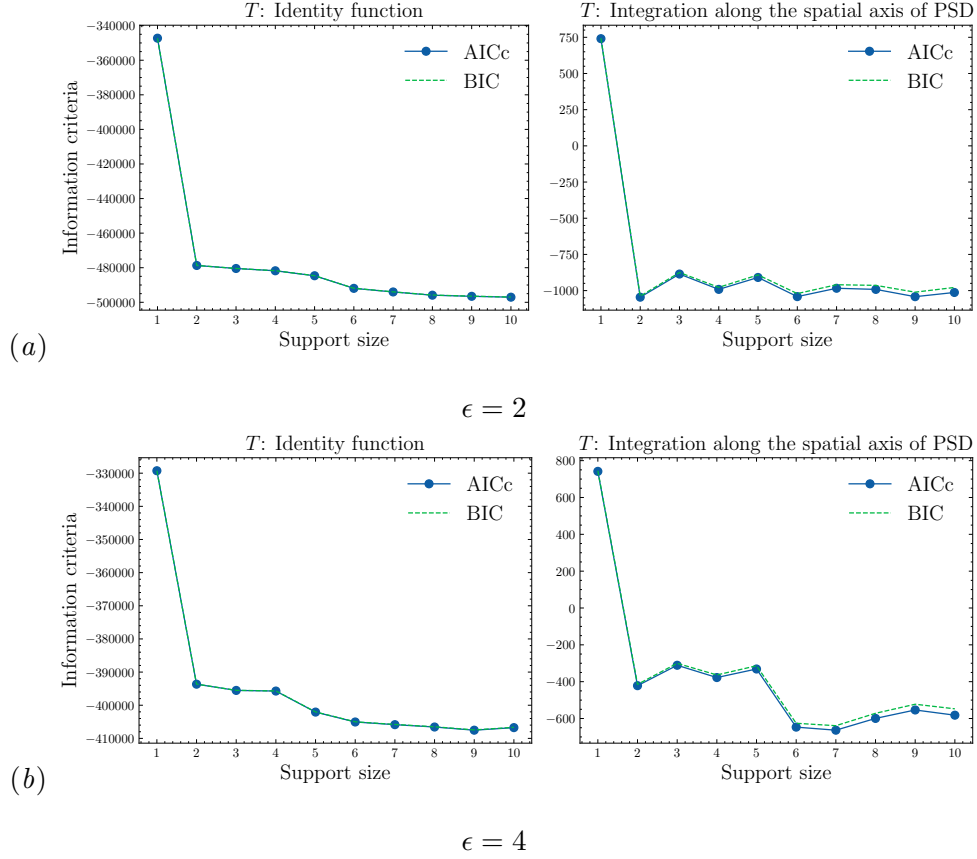


Figure 3: **Parametric Burgers' PDE**: Information criteria are calculated with different transformations  $T$ . Potential best subsets are obtained through MIOSR (not SGTR) and then validated using Equations (3). We use unnormalized  $\mathbf{U}_t^i$  and  $\mathbf{Q}^i$  when calculating RSS.

### 3.1. Parametric Burgers' PDE with Diffusive Regularization

The equation is defined with the constant diffusion of 0.1 and the time-varying coefficient  $a(t)$  for the nonlinear advection.

$$u_t = a(t)uu_x + 0.1u_{xx}; a(t) = -(1 + \frac{\sin(t)}{4}), x \in [-8, 8], \text{ and } t \in [0, 1]. \quad (6)$$

The time-dependent Burgers' equation with periodic boundary conditions is numerically solved using a spectral method on a discretized spatio-temporal grid of size  $N_x \times N_t = 256 \times 256$ . The noise-free solution  $\mathbf{U}$  (shown in the left of Figure 1) is perturbed with  $\epsilon\%$ -sd (standard deviation) Gaussian noise given by  $\epsilon \times \text{sd}(\mathbf{U}) \times \mathcal{N}(0, 1)$  to generate a noisy situation. Generally, in this work, we apply a Savitzky-Golay filter to smooth the resulting distorted data before derivative computations. The candidate terms include powers of  $u$  up to cubic order, which are multiplied by spatial derivatives of  $u$  up to fourth order. For this canonical example, PDE discovery methods are tested with  $\epsilon = 2, 4$ .

We investigate the most common method for discovering parametric PDEs, namely SGTR, and then inspect some of its problems and disadvantages. As seen in Figure 2,

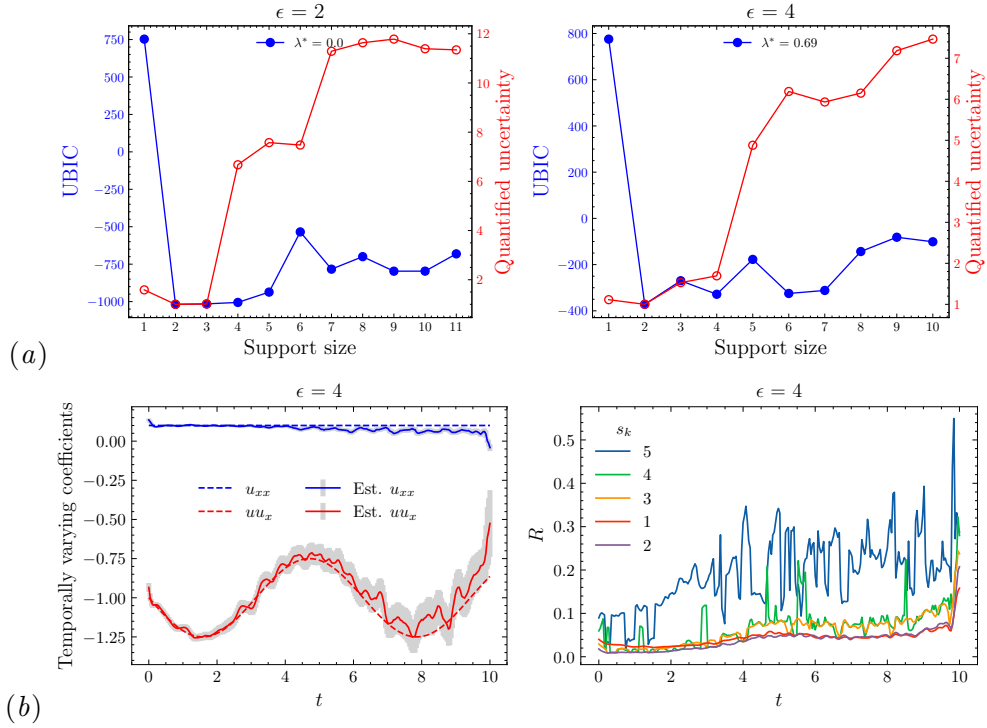


Figure 4: **Parametric Burgers' PDE:** (a) Model selection using our proposed UBIC with the PSD-based transformation under noisy situations. (b) Confidence intervals for the temporally varying coefficients and the instability (over time) of the potential PDEs with different support sizes.

in the case where the noise level is lower,  $\epsilon = 2$ , SGTR converges and identifies the true governing PDE, however, some support sizes are left unexplored, raising a concern regarding the algorithm design based on fitting Ridge solver with hard thresholding to remove small-norm coefficients iteratively. The fact that the solutions of different support sizes are not guaranteed to be optimal may have fortuitously led to the finding of the true support size. The concern turns into a real problem in the higher noise case,  $\epsilon = 4$ . Because the actual support size has never been checked by the SGTR algorithm, the false PDE is identified inevitably. Moreover, the model selection guided by the AICc loss has led us to an overfitted model anyway, as the number of training samples is large.

Considering a sequence of models with consecutive support size (no skip) obtained through MIOSR to satisfy Equation (3), we test whether our transformation  $T$  on  $\mathbf{U}_t$  and  $\mathbf{Q}\hat{\mathbf{E}}$  alleviate the overfitting problem. As seen in Figure 3, when  $\epsilon = 2$ , our PSD-based transformation is able to prevent selecting overfitted models and help us identify the governing model, while the beneficial effect is attenuated due to the higher noise level of  $\epsilon = 4$ . It is noteworthy that without any transformation ( $T$  is an identity function), we cannot at all prevent the overfitting problem.

In Figure 4(a), we test our proposed UBIC with the PSD-based transformation in identifying the governing equation. Under both noisy levels, the quantified uncertainty  $\mathfrak{U}$  is able to

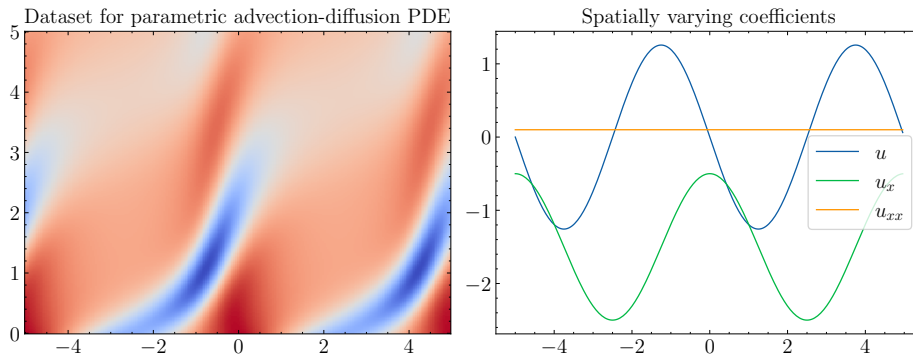


Figure 5: Visualization of the state variable and the spatially varying coefficients for the parametric advection-diffusion PDE dataset.

determine the true support size—2 for this canonical PDE. Consequently, it is natural that the UBIC utilizes the quantified uncertainty to penalize overfitted models and successfully identify the correct form of the governing Burgers’ equation despite the high noise level. In Figure 4(b), we plot the posterior coefficient and (double) standard deviation derived from Bayesian ARD regression, illustrating the 95% confidence interval. The confidence interval pinpoints when noticeable instability in the estimated posterior coefficient increases. In this case, a common behavior observed over different support sizes is the increasing instability over time steps, indicating the challenge in estimating varying coefficients (and also uncovering their symbolic expressions in Appendix A) over an extended time period. The observation suggests that long-range approximations should be circumvented to reveal the overall pattern of the varying coefficients accurately and maintain bounded instability. In Appendix A, we also employ symbolic regression to accurately recover the varying coefficients in closed form for each PDE dataset we experiment with.

### 3.2. Spatially Dependent Advection-Diffusion (AD) PDE

The advection-diffusion PDE describes the transport of a physical quantity in a varying velocity field with diffusion. We experiment with the following equation with a spatially dependent velocity:

$$u_t = c'(x)u + c(x)u_x + 0.1u_{xx}; c(x) = -1.5 + \cos\left(\frac{2\pi x}{5}\right), x \in [-5, 5], \text{ and } t \in [0, 5]. \quad (7)$$

We use a spectral method to numerically solve the PDE on a periodic domain of size  $N_x \times N_t = 256 \times 256$ . The clean solution is depicted in Figure 5. The candidate library consists of powers of  $u$  up to cubic, which are multiplied by spatial derivatives of  $u$  up to fourth order. For this PDE we also experiment with the two noise levels:  $\epsilon = 2$  and  $\epsilon = 4$ .

Considering the  $\epsilon = 2$  case in Figure S1 (‘S’ refers to a figure in the Supplementary material), the SGTR algorithm can discover the governing equation, possibly because of the suboptimal ridge solutions being compared. However, in the higher noise case,  $\epsilon = 4$ , the overfitted PDE with 4 nonzero terms is chosen instead, as favored by the AICc loss.

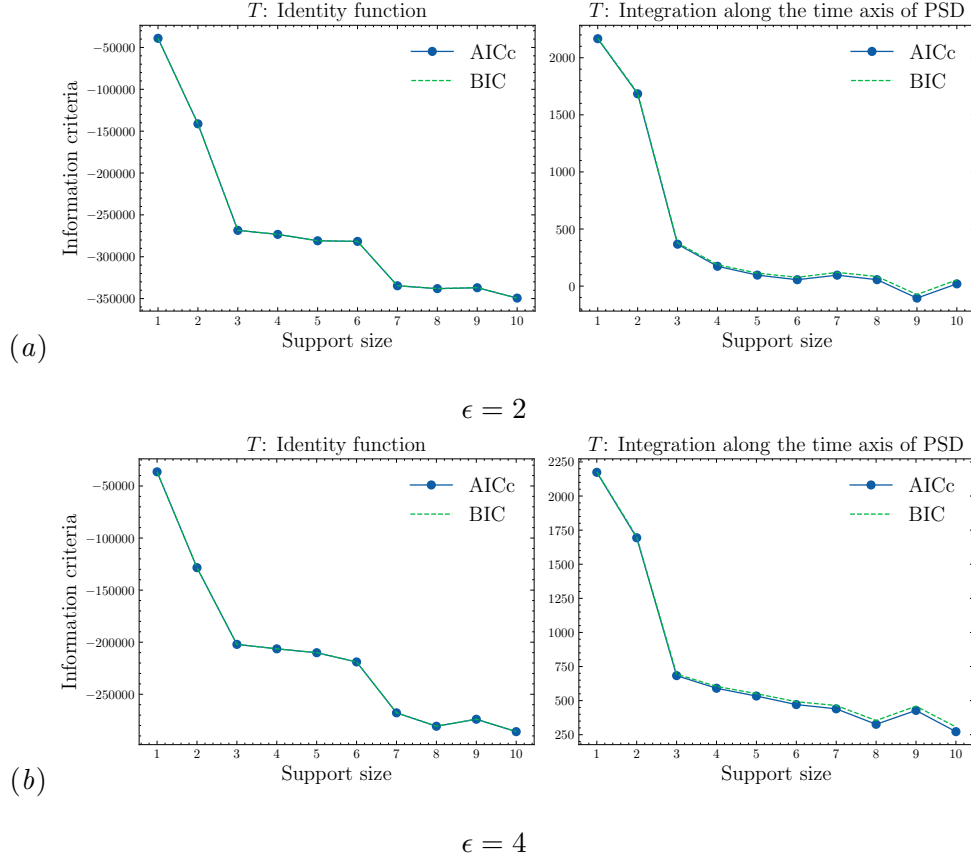


Figure 6: **Parametric advection-diffusion PDE**: Information criteria are calculated with different transformations  $T$ . Potential best subsets are obtained through MIOSR and then validated using Equations (3). We use unnormalized  $\mathbf{U}_t^i$  and  $\mathbf{Q}^i$  when calculating RSS.

As seen in Figure 6, although the overfitting problem is not completely solved, it is partially mitigated because the inclination to choose overly complicated PDEs diminishes after applying the PSD-based transformation. This observation aligns with the fact that, in the lower noise case,  $\epsilon = 2$ , the SGTR algorithm would discover an overfitted PDE instead if the L2-normalization has not been done on  $\mathbf{U}_t^i$  and  $\mathbf{Q}^i$ .

We quantify the PDE uncertainty of potential parametric models whose support size is up to 10. For the  $\epsilon = 2$  case in Figure 7(a), the quantified uncertainty points exactly to the PDE with the correct form and support size, enabling us to determine the governing equation using the UBIC. For the  $\epsilon = 4$  case, although the 3-support-size parametric model exhibits the second minimum uncertainty, it is still useful for the UBIC to identify the parametric model as the governing equation because it outperforms the 2-support-size in terms of RSS. We do not find any sufficient significance in adding more candidate terms.

In Figure 7(b), the posterior coefficient and standard deviation are plotted to illustrate the 95% confidence interval. The instability of the varying coefficients is revealed particularly near the left spatial boundary and dynamically changing locations. This observation can help refine the quantified PDE uncertainty by avoiding these dynami-

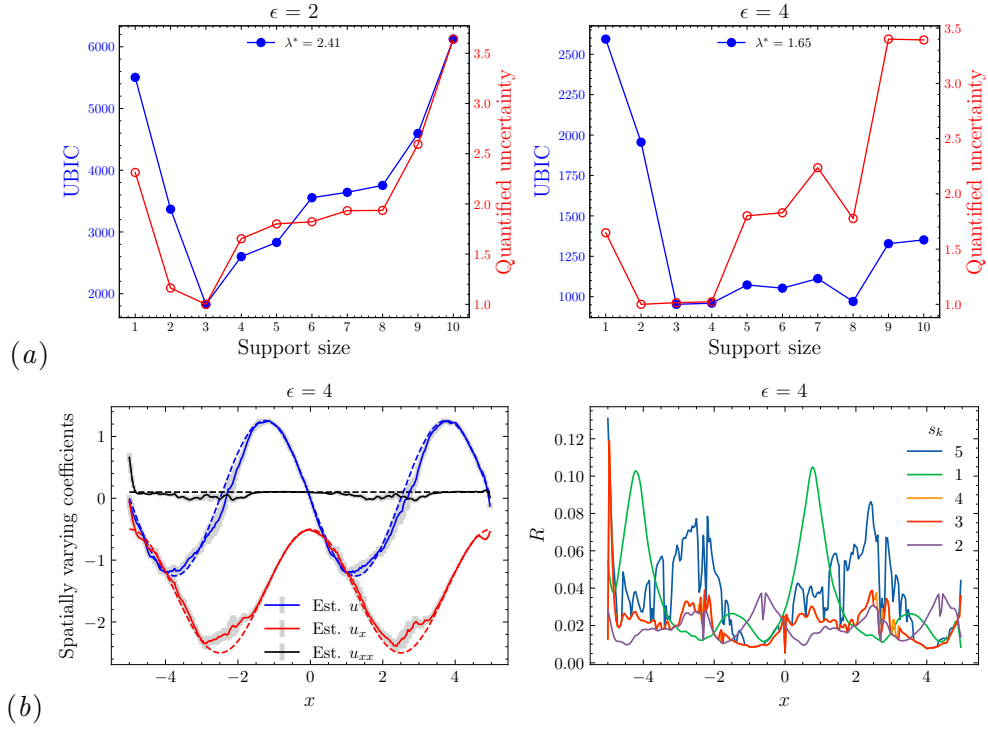


Figure 7: **Parametric advection-diffusion PDE**: (a) Model selection using our proposed UBIC with the PSD-based transformation under noisy situations. (b) Confidence intervals for the spatially varying coefficients and the instability (over spatial points) of the potential PDEs with different support sizes. Dotted lines (---) denote the true varying coefficients.

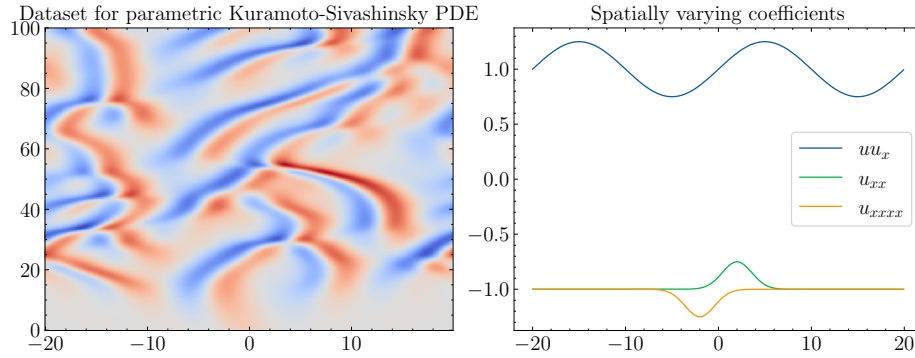


Figure 8: Visualization of the state variable and the spatially varying coefficients for the parametric Kuramoto-Sivashinsky PDE dataset.

cally changing locations. For example, considering the spatial locations starting from  $x = -5 + 4\Delta x = -4.84375$  only, the refined PDE uncertainty of the 3-support-size parametric model becomes the minimum value.

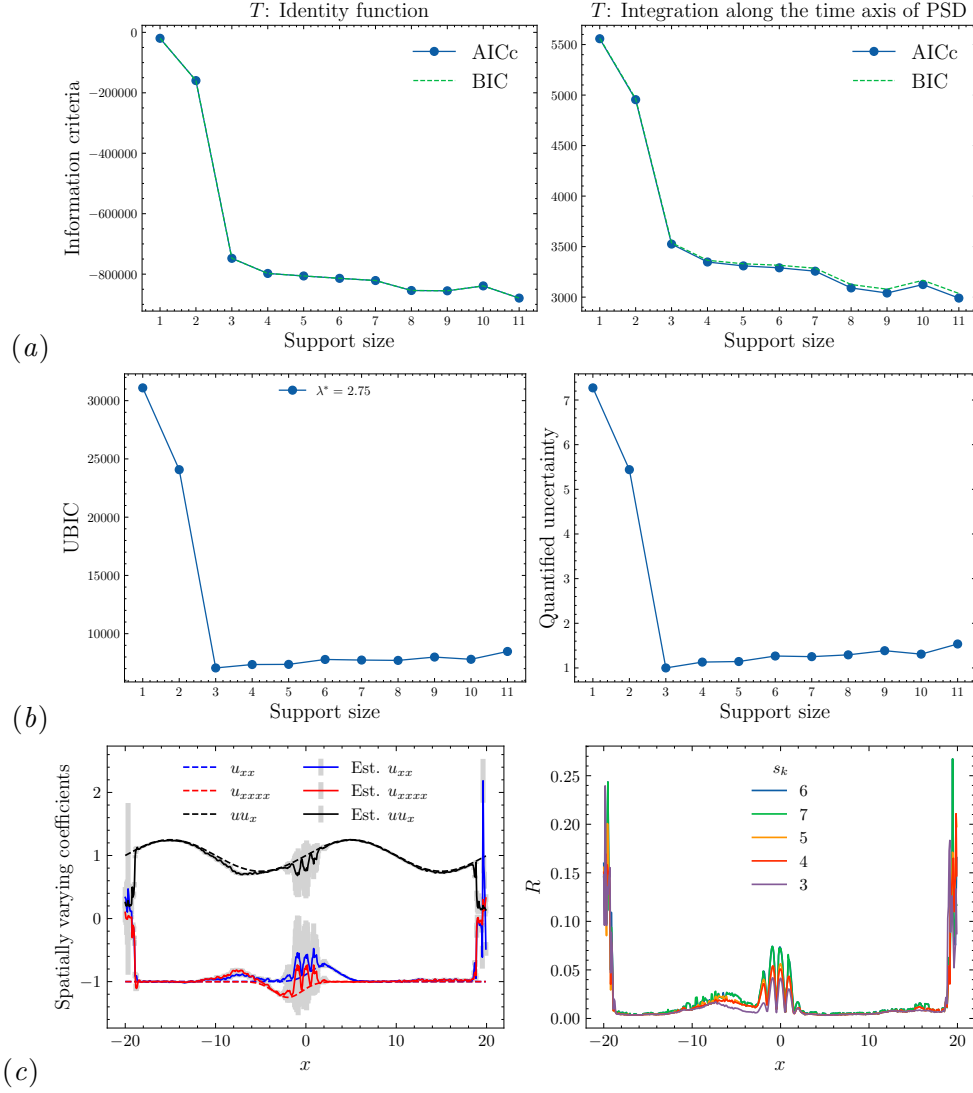


Figure 9: **Parametric Kuramoto-Sivashinsky PDE.** (a) Under the noisy situation, where we set  $\epsilon = 0.01$ , conventional information criteria are calculated with different transformations  $T$ . Potential best subsets are obtained through MIOSR and then validated using Equations (3). We use unnormalized  $\mathbf{U}_t^i$  and  $\mathbf{Q}^i$  when calculating RSS. (b) Model selection using our proposed UBIC with the PSD-based transformation under the same noisy situation. (c) Confidence intervals for the spatially varying coefficients and the instability (over spatial points) of the potential PDEs with different support sizes.

### 3.3. Spatially Dependent Kuramoto-Sivashinsky (KS) PDE

The equation has a fourth-order derivative, making its identification very challenging because of the difficulty in obtaining an accurate estimation of the fourth-order derivative, especially in noisy situations. The equation reads as follows:

$$\begin{aligned}
& u_t = a(x)uu_x + b(x)u_{xx} + c(x)u_{xxx}; \\
& a(x) = 1 + 0.25 \sin\left(\frac{2\pi x}{20}\right), \quad b(x) = -1 + 0.25e^{-\frac{(x-2)^2}{5}}, \quad c(x) = -1 - 0.25e^{-\frac{(x+2)^2}{5}}, \quad (8) \\
& x \in [-20, 20], \text{ and } t \in [0, 100].
\end{aligned}$$

The chaotic equation is numerically solved up to  $t = 200$  using  $N_x = 512$  and  $N_t = 1024$ . To limit the number of samples in our candidate library, we utilize the first half of the dataset in time (up to  $t = 100$ ), as visualized in Figure 8. The candidate library includes powers of  $u$  up to cubic, multiplied by spatial derivatives of  $u$  up to fourth order. We conduct experiments with a noise level of  $\epsilon = 0.01$ , relatively large for the noise-sensitive solution.

We find that the SGTR approach fails to discover the governing equation due to contaminated noise as well as the AICc loss, which unfortunately does not prefer parsimonious PDEs, as shown in Figure S2. It is worth introducing an additional penalty after applying the PSD-based transformation since it allows us to distinguish the BIC, computed with a greater complexity penalty, from the AICc, as seen in Figure 9(a).

In Figure 9(b), despite the noisy and problematic situation, the UBIC is able to discover the governing form successfully owing to the guiding quantified PDE uncertainty, displaying a closely identical pattern that prefers the 3-support-size (correct) parametric PDE. In Figure 9(c), the instability (over spatial points) is high around the Gaussian humps complicates the identification of the true symbolic structure underlying the spatially varying coefficients. More details are provided in Appendix A.

#### 4. Conclusion

We propose a new extension of the UBIC for solving parametric PDE problems. The extended UBIC, computed with the PSD-based transformation, leverages accumulated PDE uncertainty to overcome the overfitting problem in the model selection step, successfully disambiguating the true governing parametric PDE from overfitted PDEs with dispensable candidate terms. Through extensive numerical experiments on the three canonical PDEs, we demonstrated the noise robustness and accuracy of our method in identifying the correct number of effective terms and their varying coefficients, which represent the parametric dependencies of the governing PDE. Our results suggest that the extended UBIC is a powerful criterion for parametric PDE discovery, emphasizing the parsimony of governing equations. The ability to compute confidence intervals for varying coefficients further enhances the interpretability of potential models, providing comprehensive insights into their stability. This work not only advances the methodology for PDE discovery but also establishes a fundamental framework applicable to a wide range of complex dynamical systems. To improve the practicality of our method, we plan to use the proposed UBIC as the fitness function in a genetic algorithm based PDE discovery framework, freeing ourselves from the overcompleteness assumption on the initialized candidate library.

## References

- H. Akaike. A new look at the statistical model identification. *IEEE Transactions on Automatic Control*, 19(6):716–723, 1974. doi: 10.1109/TAC.1974.1100705.
- Dimitris Bertsimas and Wes Gurnee. Learning sparse nonlinear dynamics via mixed-integer optimization. *Nonlinear Dynamics*, 111(7):6585–6604, 2023.
- Hamparsum Bozdogan and Dominique M.A. Haughton. Informational complexity criteria for regression models. *Computational Statistics & Data Analysis*, 28(1):51–76, 1998. ISSN 0167-9473. doi: [https://doi.org/10.1016/S0167-9473\(98\)00025-5](https://doi.org/10.1016/S0167-9473(98)00025-5). URL <https://www.sciencedirect.com/science/article/pii/S0167947398000255>.
- Kevin René Broløs, Meera Vieira Machado, Chris Cave, Jaan Kasak, Valdemar Stentoft-Hansen, Victor Galindo Batanero, Tom Jelen, and Casper Wilstrup. An approach to symbolic regression using feyn. *arXiv preprint arXiv:2104.05417*, 2021.
- Steven L Brunton, Joshua L Proctor, and J Nathan Kutz. Discovering governing equations from data by sparse identification of nonlinear dynamical systems. *Proceedings of the national academy of sciences*, 113(15):3932–3937, 2016.
- Miles Cranmer. Interpretable Machine Learning for Science with PySR and SymbolicRegression.jl, 2023.
- Xin Dong, Yu-Long Bai, Yani Lu, and Manhong Fan. An improved sparse identification of nonlinear dynamics with akaike information criterion and group sparsity. *Nonlinear Dynamics*, 111(2):1485–1510, 2023.
- Amin Ghadami and Bogdan I. Epureanu. Data-driven prediction in dynamical systems: recent developments. *Philosophical Transactions of the Royal Society A: Mathematical, Physical and Engineering Sciences*, 380(2229):20210213, 2022. doi: 10.1098/rsta.2021.0213. URL <https://royalsocietypublishing.org/doi/abs/10.1098/rsta.2021.0213>.
- Seth M. Hirsh, David A. Barajas-Solano, and J. Nathan Kutz. Sparsifying priors for bayesian uncertainty quantification in model discovery. *Royal Society Open Science*, 9(2):211823, 2022. doi: 10.1098/rsos.211823. URL <https://royalsocietypublishing.org/doi/abs/10.1098/rsos.211823>.
- Clifford M. Hurvich and Chih-Ling Tsai. Regression and time series model selection in small samples. *Biometrika*, 76(2):297–307, 06 1989. ISSN 0006-3444. doi: 10.1093/biomet/76.2.297. URL <https://doi.org/10.1093/biomet/76.2.297>.
- Jun Li, Gan Sun, Guoshuai Zhao, and H Lehman Li-wei. Robust low-rank discovery of data-driven partial differential equations. In *Proceedings of the AAAI Conference on Artificial Intelligence*, volume 34, pages 767–774, 2020.
- Yingtao Luo, Qiang Liu, Yuntian Chen, Wenbo Hu, Tian Tian, and Jun Zhu. Physics-guided discovery of highly nonlinear parametric partial differential equations. In *Proceedings of*

- the 29th ACM SIGKDD Conference on Knowledge Discovery and Data Mining*, pages 1595–1607, 2023.
- David JC MacKay et al. Bayesian nonlinear modeling for the prediction competition. *ASHRAE transactions*, 100(2):1053–1062, 1994.
- N. M. Mangan, J. N. Kutz, S. L. Brunton, and J. L. Proctor. Model selection for dynamical systems via sparse regression and information criteria. *Proceedings of the Royal Society A: Mathematical, Physical and Engineering Sciences*, 473(2204):20170009, 2017. doi: 10.1098/rspa.2017.0009. URL <https://royalsocietypublishing.org/doi/abs/10.1098/rspa.2017.0009>.
- Samuel Rudy, Alessandro Alla, Steven L. Brunton, and J. Nathan Kutz. Data-driven identification of parametric partial differential equations. *SIAM Journal on Applied Dynamical Systems*, 18(2):643–660, 2019. doi: 10.1137/18M1191944. URL <https://doi.org/10.1137/18M1191944>.
- Samuel H Rudy, Steven L Brunton, Joshua L Proctor, and J Nathan Kutz. Data-driven discovery of partial differential equations. *Science Advances*, 3(4):e1602614, 2017.
- Gideon Schwarz. Estimating the dimension of a model. *The annals of statistics*, pages 461–464, 1978.
- Pongpisit Thanasutives and Ken-ichi Fukui. On uncertainty-penalized bayesian information criterion, 2024. URL <https://arxiv.org/abs/2404.16881>.
- Pongpisit Thanasutives, Takashi Morita, Masayuki Numao, and Ken-ichi Fukui. Noise-aware physics-informed machine learning for robust pde discovery. *Machine Learning: Science and Technology*, 4(1):015009, Feb 2023. doi: 10.1088/2632-2153/acb1f0. URL <https://dx.doi.org/10.1088/2632-2153/acb1f0>.
- Pongpisit Thanasutives, Takashi Morita, Masayuki Numao, and Ken-ichi Fukui. Adaptive uncertainty-penalized model selection for data-driven pde discovery. *IEEE Access*, 12:13165–13182, 2024. doi: 10.1109/ACCESS.2024.3354819.
- Peter Welch. The use of fast fourier transform for the estimation of power spectra: A method based on time averaging over short, modified periodograms. *IEEE Transactions on audio and electroacoustics*, 15(2):70–73, 1967.
- Hao Xu, Dongxiao Zhang, and Junsheng Zeng. Deep-learning of parametric partial differential equations from sparse and noisy data. *Physics of Fluids*, 33(3):037132, 03 2021. ISSN 1070-6631. doi: 10.1063/5.0042868. URL <https://doi.org/10.1063/5.0042868>.

## Appendix A. Symbolic discovery of varying coefficients

Symbolic discovery of varying coefficients is achieved via the PySR package (Cranmer, 2023). To prioritize parsimonious expressions of varying coefficients, we consider model rankings based on the PySR’s score. We evaluate any selected interpretable expression  $\hat{h}(x)$  against its ground truth  $h(x)$  using the percentage relative coefficient error:  $\text{CE}(h(x), \hat{h}(x)) =$

Table 1: Symbolic expression of varying coefficients

Dataset	Noise level ( $\epsilon$ )	Discovered varying coefficients	%Coefficient error
Burgers	2	$0.09441, -0.98643 - 0.25067 \sin(t)$	1.286, 5.591
	4	$0.08080, -0.25146 \sin(t) - 0.95987$	19.20, 3.813
AD	2	$-\sin(1.2458x), \cos(1.2499x) - 1.4502, 0.08736$	20.05, 2.958, 12.64
	4	$-\sin(1.2415x), \cos(1.244x) - 1.4216, 0.06406$	20.06, 4.554, 35.94
KS	0.01	$0.25113 \sin(0.32253x) + 0.95955$	4.055
		$-0.976754 + 0.353986e^{-0.493521(1-0.547288x)^2}$	4.027
		$-0.966723 - 0.249388e^{-3.73627(0.429437x+1)^2}$	4.365

$100 \times \frac{\|\hat{h}(x) - h(x)\|_1}{\|h(x)\|_1}$ . We note that  $\text{CE}(h(t), \hat{h}(t))$  are calculated in the same manner. Table 1 lists the relative coefficient errors for every experiment in this paper. In the experimental cases of the parametric Burgers’ and AD PDEs, we can uncover the correct mathematical expressions/structures of the varying coefficients with acceptable accuracy. For the parametric KS PDE case, we cannot initially retrieve the correct expression only for the varying coefficient of  $u_{xxxx}$ , as the suggested expression by PySR is  $-0.9798 + 0.19909xe^{-0.26832x^2}$ , which however hints that a common Gaussian function should be used instead due to its similar accuracy. To refine the initial expressions for  $u_{xx}$  and  $u_{xxxx}$ , we use Feyn’s autorun functionality (Broløs et al., 2021) with minimal complexity settings, ultimately discovering the Gaussian formulas. The coefficient errors are satisfactory, less than 5%.

## Appendix B. Noise-robustness of PSD

We explore the noise-robustness of our PSD-based transformation using the Burgers’ PDE as an example. In Figure 10, different representations of  $\mathbf{U}_t$  are presented. We evaluate the accuracy of each representation by comparing it to the ground truth data using the relative Frobenius-norm error. The fact that our PSD-based transformed representation matches its ground truth more closely than other representations under the noisy situation demonstrates its superior robustness. Therefore, we apply our extended UBIC with the PSD-based transformation.

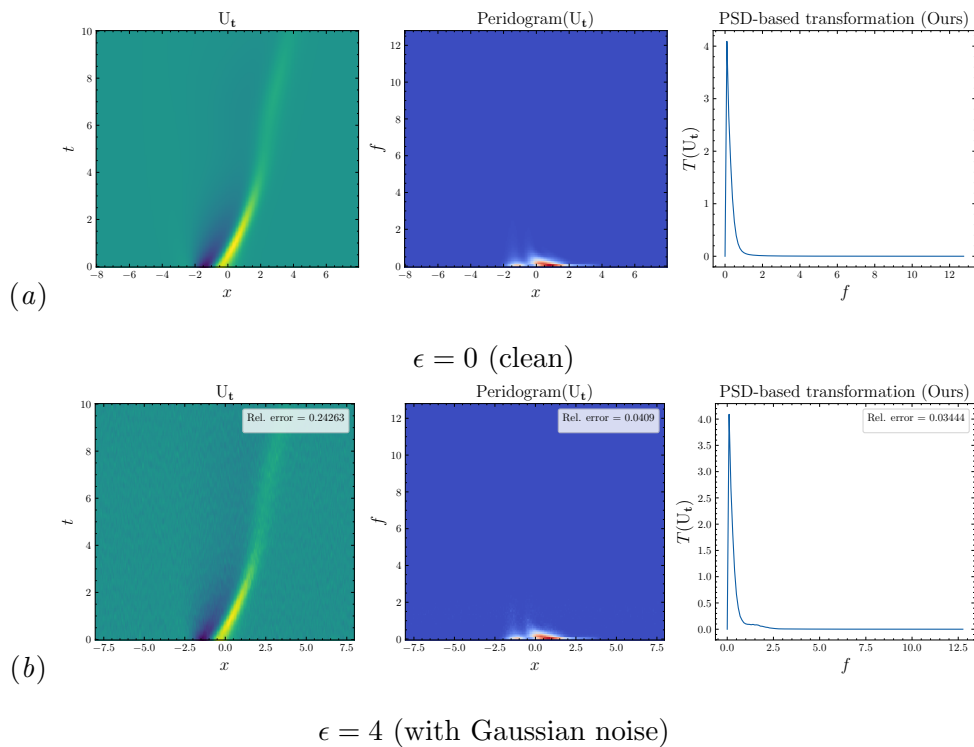


Figure 10: **Parametric Burgers' PDE.** We visualize different representations of  $U_t$  and measure their relative errors against the ground truth data.